Talbot, E.L., Berson, A., Brown, P.S. and Bain, C.D., Submitted to Physical Review E, 'Evaporation of Picolitre Droplets on Surfaces with a Range of Wettabilities and Thermal Conductivities' (accepted)

Evaporation of Picolitre Droplets on Surfaces with a Range of Wettabilities and Thermal Conductivities

E.L. Talbot[1], A. Berson[2], P.S. Brown[1] and C.D. Bain[1]

[1]*Department of Chemistry, Durham University, Durham, DH1 3LE, United Kingdom*
[2]*School of Engineering and Computing Sciences, Durham University, Durham, DH1 3LE, United Kingdom*

(Dated: June 8, 2012)

The evaporation of picolitre water and ethanol droplets generated by Drop-on-Demand inkjet printing was investigated on substrates with apparent contact angles between 10° and 135° and thermal conductivities between $0.25-149\ Wm^{-1}K^{-1}$. Drying times were calculated from a diffusion-limited model for droplets with both pinned and moving contact lines as a function of droplet diameter and apparent contact angle. Droplets with a moving contact line take longer to dry on hydrophilic substrates than pinned droplets. The difference in drying times between evaporative modes vanishes at large apparent contact angles. Hence, similar drying times are obtained for both modes on hydrophobic substrates. The predicted drying times for glass and silicon substrates were in good quantitative agreement with experimental data, suggesting that thermal effects are negligible for substrates of these base materials. However, on a PTFE substrate which has a lower thermal conductivity more relevant to inkjet printing, evaporative cooling reduces the evaporation rate causing drying times to be under-predicted by isothermal models.

PACS numbers: 68.03.Fg, 47.55.D-

I. INTRODUCTION

The evaporation of sessile droplets depends on the properties of the fluid and on the ambient atmosphere, e.g. temperature and relative humidity, but is also influenced by the characteristics of the substrate. The present study focuses on the effect of the wetting properties of the substrate on the evaporation of sessile droplets. The influence of the retraction of the contact line during drying is addressed for two limiting drying modes [1]: the constant contact angle mode, in which the droplet radius decreases with time and the contact angle remains fixed, and the constant contact area mode, wherein the contact line is pinned throughout drying. The former mode occurs on substrates with low contact angle hysteresis and is often observed on hydrophobic substrates [2]. Contact line pinning is enhanced by surface roughness, chemical heterogeneities or particles inside the droplet.

A number of studies have investigated the evaporation of microlitre droplets [3–6]. Under normal laboratory conditions (an air atmosphere at approximately 1 atm and 300 K), the evaporation rate is limited by the diffusion of vapour from the liquid-vapour interface into the ambient atmosphere. When evaporation takes place in the droplet's own vapour, or for very small droplets (∼100 nm in diameter), evaporation may be governed by the kinetics of the transfer of molecules across the interface [5]. Only diffusion-controlled evaporation is considered here.

For a partially wetting sessile droplet, the evaporative flux is not uniformly distributed along the liquid-vapour interface. The evaporative flux, which is larger near the contact line and smaller at the apex of the droplet, can be modelled by the equivalent problem of the capacitance of a lens. This problem was solved theoretically by Picknett and Bexon [1] for the full range of contact angles. Numerical models for contact angles below 90° were later established for pinned droplets by Deegan *et al.* [7] and Hu and Larson [8]. Popov [9] also proposed an analytical model for the full range of contact angles, which is similar to the model proposed by Picknett and Bexon, but can be solved without the use of an infinite series.

Theoretical drying curves [1] predict an increase of the drying time with increasing contact angle. A notable difference in drying times is also expected between pinned and de-pinning droplets at contact angles, θ, below 90°. As θ increases above 90°, the difference in drying times becomes less marked, until at $\theta \backsimeq 140°$ the drying times are similar. The diffusion-controlled model by Popov has been verified for pinned droplets [10, 11] over a large range of contact angles. Comparisons between pinned and de-pinning droplets were performed only for contact angles below 60° [3, 11].

All the aforementioned studies were performed for microlitre droplets (typically $0.5-15\ \mu L$), whereas inkjet droplets typically have picolitre volumes ($4-65\ pL$), i.e. five or six orders of magnitude smaller. To our knowledge, there are no measurements comparing the drying of picolitre droplets to a diffusion-limited model for the full range of contact angles and both limiting evaporative modes.

First, we discuss the assumptions made in modelling

the evaporation of microlitre droplets, and ask whether these assumptions are still valid for picolitre droplets. The diameter of inkjet droplets ranges between 10 μm and 100 μm. Evaporation should still be limited by diffusion at this scale.

Convection occurs in evaporating sessile droplets [12] where, in order to conserve mass, evaporating liquid is replenished by a convective flow. This convective flow is responsible for the "coffee-ring" deposits formed from droplets drying with a pinned contact line [13]. In addition, thermal or concentration gradients at the free surface of the droplet can drive Marangoni flows.

Convection can affect the evaporation rate by influencing the heat transfer inside the droplet. Kelly-Zion *et al.* [14] demonstrated that free convection has to be taken into account for very large droplets (6 mm in diameter) otherwise the evaporation rate is underestimated. For picolitre droplets however, convective heat transfer due to internal flows is negligible compared to conduction. The relative effect of convection and conduction is seen in the Péclet number, $Pe = uR/K$, where K is the thermal diffusivity of the fluid, u is the velocity and R the contact radius of the droplet. For a droplet of water ($K = 1.4 \times 10^{-7}$ m^{2}s^{-1}) with a radius $R = 25$ μm and internal velocities of the order of $u = 100$ μms^{-1}, $Pe = 0.018 \ll 1$, which means that conduction predominates.

Evaporative models for sessile droplets (e.g. [9]) usually assume that the process is isothermal. Several studies [15–19] have recently shown that this assumption breaks down when the substrate has a poor thermal conductivity. When the substrate acts as an insulator, heat transfer from the surroundings is insufficient to balance the latent heat of vaporization and the liquid in the droplet cools down. As a consequence, the saturation vapour pressure at the liquid-vapour interface decreases and evaporation slows down.

Evaporative cooling was neglected in recent studies on microlitre droplets [3, 10, 11], because the substrates (silicon wafers or aluminum plates) had large thermal conductivities. Inkjet printing often involves substrates with poor thermal conductivities such as paper, for which evaporative cooling might not be negligible. Here, we investigate whether evaporative cooling is important in the case of picolitre droplets or whether the process can still be assumed to be isothermal.

In this paper, we verify the isothermal, diffusion-controlled model by Popov on a scale relevant to inkjet printing for both pinned droplets and those with a moving contact line. This work addresses the evaporation of picolitre water droplets on a number of substrates with apparent contact angles in the range of 10° to 135° and thermal conductivities in the range $0.25 - 149$ $Wm^{-1}K^{-1}$.

II. EXPERIMENTAL

A. Evaporative Model

Picolitre droplets have Bond numbers $\ll 1$, therefore gravitational effects are negligible. Sessile droplets can be considered as a spherical cap with a mass given by

$$M = \pi\rho R^3 \frac{\cos^3\theta - 3\cos\theta + 2}{3\sin^3\theta}, \tag{1}$$

where R is the droplet radius, ρ is the liquid density, M is the droplet mass and θ is the three-phase apparent contact angle. Figure 1 indicates the relevant droplet parameters.

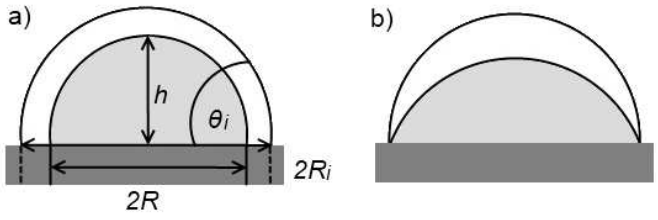

FIG. 1. Schematics for drying with a) a moving contact line with constant contact angle, and b) a pinned line. R_i is the initial radius, h is the height, R is the current radius and θ_i is the initial contact angle.

Evaporation is limited by diffusion, and diffusion is considered quasi-steady. Indeed, the time scale for the build-up of a concentration profile around the droplet by diffusion ($t_{diff} = R^2/D$ with a length scale R) is much smaller than the drying time t_{dry} (i.e. $t_{diff}/t_{dry} \ll 1$), where D is the diffusion coefficient of vapour in the ambient atmosphere. The dynamics of the droplet surface are neglected and it is assumed that at any instant the droplet has its equilibrium shape [9]. The Kelvin correction to the vapour pressure is negligible for the droplet sizes considered. Thermal effects due to evaporative cooling are also neglected, as are Marangoni effects.

The rate of mass loss over time, t, is given as [9]

$$\frac{dM}{dt} = -4\pi R(t) D (n_s - n_\infty)\left[\frac{\sin\theta(t)}{4(1+\cos\theta(t))} + \int_0^\infty \frac{1+\cosh(2\theta(t)\tau)}{\sinh(2\pi\tau)} \tanh[(\pi-\theta(t))\tau]\,\mathrm{d}\tau\right], \tag{2}$$

where n_s is the saturation vapour density and n_∞ is the ambient vapour density, given as $n_\infty = RH \times n_s$ for a relative humidity, RH. The term outside of the square bracket gives the evaporation rate for a spherical droplet. The terms inside the square bracket account for the non-uniformity of the evaporation rate along the

interface of a sessile droplet.

The time dependence of the contact angle for a pinned droplet, $R(t) = R_i$, can be obtained from combining equations 1 and 2, then solving for a constant droplet radius [9], yielding

$$\frac{d\theta(t)}{dt} = -\frac{D(n_s - n_\infty)}{\rho R_i^2}(1+\cos\theta(t))^2\left[\frac{\sin\theta(t)}{1+\cos\theta(t)} + 4\int_0^\infty \frac{1+\cosh(2\theta(t)\tau)}{\sinh(2\pi\tau)}\tanh[(\pi-\theta(t))\tau]\,\mathrm{d}\tau\right]. \tag{3}$$

Equation 3 was solved using the *ode45* function in MATLAB. The numerical integration was computed by a trapezoidal method, the *trapz* function in MATLAB. The drying time t_P of a pinned droplet is defined by the time when the contact angle reaches zero. In the limit of small contact angles, the drying time, $t_{P,\theta}$, reduces to

$$t_{P,\theta} = \frac{\pi\rho R_i^2\theta_i}{16D(n_s - n_\infty)}, \tag{4}$$

with θ_i being the initial contact angle [9].

Alternatively, equation 2 can be solved for a constant contact angle to find the time dependence of the radius for a droplet with a moving contact line, as in [12, 20], giving

$$R(t)^2 = R_i^2 - 2\frac{D(n_s - n_\infty)}{\rho}\frac{\sin^3\theta}{\cos^3\theta - 3\cos\theta + 2}\,t \left[\frac{\sin\theta}{1+\cos\theta} + 4\int_0^\infty \frac{1+\cosh(2\theta\tau)}{\sinh(2\pi\tau)}\tanh((\pi-\theta)\tau)d\tau\right]. \tag{5}$$

The drying time t_M for a droplet evaporating with a constant contact angle, is defined as the time when the radius reaches zero. Note that the square of the radius decreases linearly with time [5].

Finally, we define the drying time t_{hem} for a hemisphere with a freely moving contact line. For the hemisphere, evaporation is uniform along the interface and the drying time for a hemisphere of equivalent volume to our droplets will be used in the following for normalisation.

B. Experimental Set-up and Procedure

Picolitre droplets were ejected from a Microfab piezoelectric printhead (MJ-ABP-01, Horizon instruments) with a 50 μm orifice. The device was connected to a reservoir pressurised by a syringe. Drop-on-demand printing was controlled using a Microfab driver unit (Microfab JetDrive III Controller CT-M3-02). High-purity water (MilliQ) or ethanol filtered through a 0.45 μm pore filter were used as the fluids.

Shadowgraph profile images of the droplets were produced using side illumination. A cold LED light source (Beaglehole instruments) was chosen to prevent temperature gradients across the droplet. A 20× magnification objective (NA 0.4, WD 10 mm, Nikon MPlan) was used to magnify the images. Images were captured with a high-speed camera (Photron APX RS) at a shutter speed between 111 μs and 50 μs and a frame rate between 66 and 10,000 fps depending on the fluid and droplet characteristics. The resolution was limited by the pixel size, which was on average $\sim 0.97 \times 0.97$ μm^2. This was sufficient to resolve the end stages of drying. The relative humidity and temperature in the region of the nozzle were measured with a thermohygrometer (Extech), with maximal systematic errors associated with the calibration of the relative humidity, RH ±4% and temperature, T ±1 K respectively. The entire set-up was contained within a box to reduce air currents and limit convective cooling.

Shadowgraph images were post-processed in MATLAB using an automated routine to subtract the background, convert to binary and fill in droplet reflections (see supplementary information for example images). The droplet height was measured by summing the largest number of pixels in the vertical direction. The diameter was measured by summing the number of pixels along the droplet baseline. The volume, V, and contact angle, θ, were then calculated for a spherical cap:

$$V = \frac{\pi h}{6}\left(3R^2 + h^2\right) \tag{6}$$

and

$$\theta = 2\tan^{-1}\left(\frac{2h}{R}\right), \tag{7}$$

where R is the radius of the contact area and h is the apex height.

Contact angles from microlitre water droplets (∼1.0 μL) were measured using a video capture system (AST Products, VCA250XE) and related software (VCA 2500 (Version 1.12a), AST Products). Droplets were gently placed on the substrate for measurement by drop shape analysis.

C. Sample Preparation

A number of substrates were prepared to provide a range of wettabilities. Glass microscope slides were given different treatments. First, substrate G was simply wiped with lint-free tissue. Second, substrate RG was rinsed with high purity water (MilliQ). Third, substrate DG was left overnight in 2%(w/w) decon 90 alkaline cleaning

solution, before rinsing with high purity water. Rinsed substrates were dried in nitrogen and left in an oven to ensure full drying. PTFE substrates were prepared in the same manner as substrate G.

Substrate VBC was a glass slide placed in an evacuated plasma chamber and exposed to vinylbenzylchloride monomer [21] (Sigma Aldrich +97% purity) at a flow rate of 1.6 x 10^{-7} kgs^{-1} with a pressure of 0.2 mbar. Purging for 5 minutes was followed by ignition of the electrical discharge. The pulse duty cycle consisted of 100 μs on and 4 ms off. The radio frequency used was 13.56 MHz. Plasma deposition was for a duration of 1 minute, followed by 5 minutes of quenching.

Substrates S1, S2, S3 and S4 were silicon wafers spin-coated with polybutadiene solution in toluene before undergoing plasmachemical fluorination [22] with CF_4 gas (Air products, 99.7% purity). S1 and S2 were treated at a power of 30 W and 10 W respectively for 10 minutes. S3 and S4 were treated at 10 W for 5 minutes at different locations in the reactor, resulting in different roughnesses. S1 showed a root mean squared (rms) roughness of ∼130 nm by AFM (Digital Instruments Nanoscope III scanning probe microscope), whereas S2 had an RMS roughness of ∼90 nm. S3 and S4 had rms roughnesses of ∼95 nm and ∼75 nm respectively. All four substrates had the same surface chemistry (measured by XPS) but different surface roughness.

The substrate base materials were chosen to give a range of thermal conductivities in order to examine the effects of evaporative cooling on the evaporation rate. Substrates with a silicon wafer base had a high thermal conductivity, while PTFE gave a low thermal conductivity (table I.).

TABLE I. Thermal conductivities, κ, of the substrates.

Base Material	Substrates	κ / $Wm^{-1}K^{-1}$
PTFE	PTFE	0.25
Glass	DG, RG, G, VBC	0.96
Silicon	S1, S2, S3, S4	149

III. RESULTS AND DISCUSSION

Typical contact angles from microlitre droplets and picolitre droplets on each substrate are compared in table II. Example image sequences for drying droplets are shown in Fig. 2 with corresponding videos in the supplementary information. Water droplets drying on substrates VBC, S1, S2, S3 and G dried with a pinned contact line. On substrates DG, RG, PTFE and S4, water droplets dried with a moving contact line. The actual drying behaviour was intermediate between the two limiting modes (see S4 in Fig. 2). The drying mode was categorised as closest to the pinned mode if the droplet diameter varied by 25% or less in 85% of the drying time. Ethanol droplets were deposited only on substrates S3, S4 and PTFE. In each case, ethanol droplets dried with a moving contact line.

TABLE II. A comparison of contact angles post-spreading for microlitre and picolitre water droplets on the same substrate.

Substrate	θ μL drop	θ pL drop	Drying Mode
DG	17°± 6°	14°± 2°	Moving
RG	24°± 7°	15°± 3°	Moving
G	33°± 7°	40°± 10°	Pinned
PTFE	108°± 1 °	100°± 3°	Moving
VBC	80°± 2°	65°± 6°	Pinned
S1	174°± 2°	133°± 8°	Pinned
S2	173°± 2°	130°± 3°	Pinned
S3	130°± 1°	118°± 1°	Pinned
S4	118°± 1°	109°± 1°	Moving

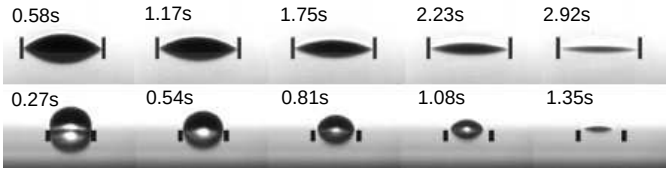

FIG. 2. Example image sequences for a pinned water droplet drying on substrate G (top), and for a water droplet drying on S4 with a moving contact line (bottom). Vertical lines indicate the initial position of the contact line.

On all substrates with the exception of G, the observed apparent contact angles for the picolitre droplets were smaller than for microlitre droplets. This difference is beyond the scope of this paper, but may result from the influence of the droplet scale compared to microscopic features on the substrate [23], or it may be due to impact [24]. In our model, the evaporative flux depends on the shape of the droplet. Therefore, the necessary input for the initial contact angle in the model is the apparent contact angle at the picolitre scale. Note that the actual thermodynamic contact angle involved in the Young-Laplace equation never appears in the model.

The results for picolitre droplets in each contact-angle regime (above and below 90°) and for each drying mode (pinned and moving contact line) are shown in Figs. 3, 4 and 5 for water droplets on the substrates VBC, S2, and S4, and for ethanol droplets on S4. Data from five or more droplets were collected on each substrate. For easier readability, the trends shown in Figs. 3, 4 and 5 are for one representative droplet on each substrate only.

The evolution of the droplet diameter and contact angle with time are presented in Figs. 3 and 4. The diameters of water droplets drying on substrates VBC and S2 remain pinned for most of the droplet lifetime. On substrate S4, water and ethanol droplets dried with a

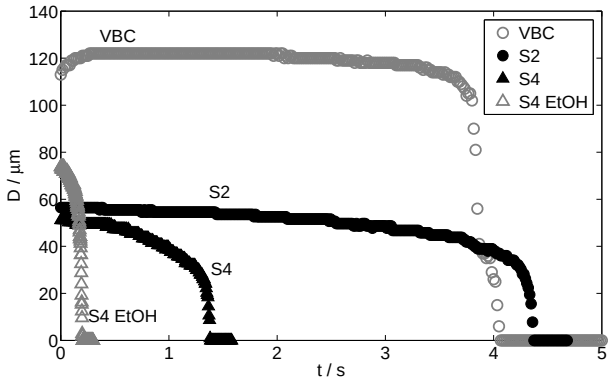

FIG. 3. Typical evolution of droplet diameters during the drying lifetime for each drying regime. ○: pinned drying, △: moving contact line. Closed symbols represent contact angles $> 90^\circ$ and open symbols represent $< 90^\circ$.

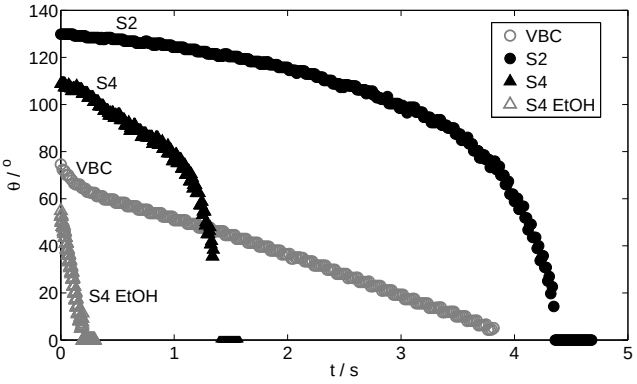

FIG. 4. The evolution of droplet contact angles during drying. ○: pinned drying, △: moving contact line. Closed symbols represent contact angles $> 90^\circ$ and open symbols represent $< 90^\circ$.

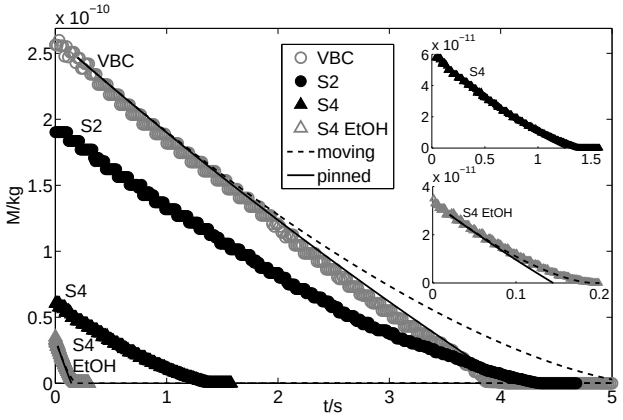

FIG. 5. The mass loss rate during the drying lifetime. ○: pinned drying, △: moving contact line. Closed symbols represent contact angles $> 90^\circ$ and open symbols represent $< 90^\circ$. Inserts show evaporation on substrate S4 with water above and ethanol below.

moving contact line, although the contact angle was not constant. Some droplets show an initial increase in their diameter, which corresponds to the end of spreading. The part of the signals corresponding to the end of spreading is discarded by removing the first 0.2 s of the datasets for water droplets and the first 0.02 s for ethanol.

TABLE III. The predicted drying times for the moving contact line regime t_M, the pinned contact line regime t_P and the pinned regime in the limit of small contact angles $t_{P,\theta}$, compared to the experimental drying time, t_{exp}, for each substrate. Drying times for droplets on each substrate are for a single representative droplet. Fluid type is indicated by w for water and e for ethanol. Temperatures ranged between 293.5 K and 295.0 K.

Surface, fluid	t_{exp}/s	$t_{P,\theta}$/s	t_P/s	t_M/s	RH
G, w	3.03	2.92	2.95	4.06	0.59
RG, w	0.57	0.47	0.47	0.6	0.47
DG, w	2.18	1.85	1.83	2.61	0.50
PTFE, w	3.21	1.61	2.39	2.72	0.49
PTFE, e	0.18	0.10	0.10	0.13	0.00
VBC, w	3.93	3.67	4.07	5.27	0.48
S1, w	4.09	1.65	4.18	4.34	0.50
S2, w	4.36	1.76	4.22	4.41	0.50
S3, w	1.46	0.85	1.40	1.53	0.26
S4, w	1.40	0.87	1.27	1.42	0.26
S3, e	0.24	0.16	0.17	0.23	0.00
S4, e	0.19	0.14	0.14	0.19	0.00

The results of the theoretical model for substrates with base materials of glass or silicon are in good agreement with the experimental data, both quantitatively (table III) and in the shape of the mass loss rate (Fig. 5), despite any intermediate behaviour between limiting regimes. The drying mode was always intermediate to some extent as the droplets did not stay fully pinned or with a perfectly constant contact angle during their whole lifetime. However, the drying times remained close to the limiting-mode predictions. Our results confirm the validity of the diffusion-controlled isothermal evaporation model in the picolitre regime on substrates with thermal conductivities of 1 $Wm^{-1}K^{-1}$ or higher. The model has no fitting parameter, which makes it particularly suitable for predicting the drying time of inkjet droplets.

In contrast, on the low conductivity PTFE substrate the drying times are under-predicted by the model due to evaporative cooling slowing the evaporation. Estimates of the degree of evaporative cooling were made by adjusting the temperature input to the model in order to best fit the experimental data. Temperature differences from ambient conditions for droplets on the PTFE substrates were estimated at $\sim 2.7\pm1$ K for water droplets on PTFE and $\sim 5.8\pm1$ K for ethanol droplets on PTFE. The magnitudes of these estimates agree well with experimental values reported in [18] for microlitre droplets. Hence, the

model cannot be used for predictions of the drying time on substrates with thermal conductivities lower than that of glass, as the isothermal assumption does not hold.

For droplets with initial contact angles below 90°, pinned droplets show a linear mass loss rate, represented in Figure 5 by drying on VBC (○). In contrast, droplets with a moving contact line, demonstrated on S4 with ethanol (△), exhibit a decrease in the mass loss rate towards the end of drying. The drying times for droplets of equal volume on hydrophilic substrates can vary significantly depending on whether the contact line is pinned or moving. It is interesting to note that both evaporative modes behave similarly during the initial stage of evaporation and diverge only towards the end of drying. The dependence of the drying time on the late stages of drying could prove especially important for transitory modes or stick-slip motion [3], where the droplet de-pins part way through drying. As there is little dependence of the drying time on the drying mode for the initial stages of drying, early de-pinning will give drying times corresponding to droplets drying with a moving contact line. In contrast, late transitions in the drying mode or stick-slip motion may give behaviour in-between the pinned and de-pinning predictions.

At large contact angles (approximately $\theta > 90°$), the mass loss rate becomes non-linear for both drying modes. The difference in the drying time between constant contact angle and constant contact area modes decreases, until at a contact angle of approximately 140° the drying times are very similar (Fig. 6). Therefore, for hydrophobic surfaces, the dependence of the drying time on the drying mode is much less than on hydrophilic substrates.

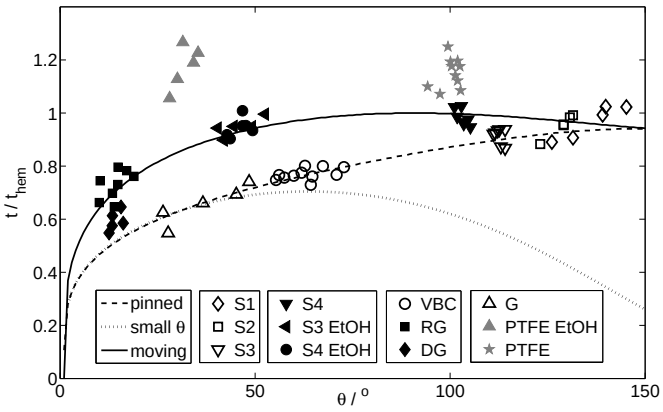

FIG. 6. The drying times are plotted for each drying mode, normalised by the time for a free hemisphere of the same volume to dry. Open symbols indicate pinned drying, filled symbols indicate a moving contact line. The contact angle used is at 0.2 s for water and 0.02 s for ethanol to ensure spreading has ended.

Figure 6 shows the drying times predicted by the theoretical model. Drying times are normalised by t_{hem}, the drying time of a hemisphere of equal volume with a freely moving contact line. The agreement between the predicted drying times and the experimental ones is very good for both fluids on glass and silicon substrates, further validating the model for picolitre droplets on substrates with thermal conductivities of 1 $Wm^{-1}K^{-1}$ or above. For droplets deposited on PTFE substrates, with lower thermal conductivity, the experimental drying times deviate from the model predictions as a result of evaporative cooling. Small-angle predictions (equation 4) are in agreement with the experiment for contact angles below 45°, but fail above 45° as expected. The drying time for the pinned contact-line mode increases with apparent contact angle until predictions coincide with the model curve for the moving contact-line mode.

IV. CONCLUSION

Diffusion-limited evaporative models have previously been validated for microlitre droplets, but not for picolitre droplets considering a full range of contact angles and limiting evaporative modes. Picolitre droplets of water and ethanol on substrates with thermal conductivities $\geq$ 1 $Wm^{-1}K^{-1}$ follow a diffusion-limited isothermal evaporative model [9]. The model has been verified on these substrates for contact angles ranging between 10° and 135°. In addition, the model successfully captures the two limiting modes of evaporation. The drying time is dependent on both the substrate hydrophobicity and the drying mode. Pinned droplets dry faster than those with a moving contact line, and evaporation on hydrophilic substrates is faster than on hydrophobic substrates. The difference between drying times for each drying mode is more pronounced for contact angles below 90°.

The model and experimental measurements are in good agreement for substrates of silicon or glass, allowing drying times to be predicted accurately for both evaporation modes on substrates with thermal conductivities $\geq$ 1 $Wm^{-1}K^{-1}$. Such estimates of the drying times could be particularly useful in applications such as spray cooling, where the rate of evaporation must be critically controlled. The only input parameters are the thermophysical properties of the fluid and surrounding atmosphere, the ambient conditions (temperature and relative humidity) and the apparent radius and contact angle of the droplet. No fitting parameter is required.

Glass marks the threshold for thermal conductivity below which evaporative cooling is no longer negligible. On lower conductivity substrates ($\kappa \leq 1$ $Wm^{-1}K^{-1}$) such as PTFE, the evaporation rate is slowed significantly due to evaporative cooling. As a consequence, the isothermal model breaks down, under-predicting the drying time. A more complex model including energy balances is needed to account for evaporative cooling. This conclusion has implications for inkjet printing, where low conductivity paper substrates are common.

ACKNOWLEDGMENTS

The authors are grateful to J.P.S. Badyal for making his facilities available for the fabrication of substrates. This work was supported financially by EPSRC under grant number EP/H018913/1.

[1] R.G. Picknett and R. Bexon, J. Colloid Interface Sci. **61**, 2, 336–350, (1977).

[2] D.H. Shin, S.H. Lee, J. Jung, and J.Y. Yoo, Microelectron. Eng. **86**, 4-6, 1350–1353, (2009).

[3] M. Shanahan, K. Sefiane, and J. Moffat, Langmuir **27**, 8, 4572–4577, (2011).

[4] S. Rowan, M. Newton, and G. McHale, J. Phys. Chem. **99**, 35, 13268–13271, (1995).

[5] A.M. Cazabat and G. Guéna, Soft Matter **6**, 12, 2591–2612, (2010).

[6] N. Murisic and L. Kondic, J. Fluid Mech. **679**, 219–246, (2011).

[7] R. Deegan, O. Bakajin, T. Dupont, G. Huber, S. Nagel, and T. Witten, Phys. Rev. E **62**, 1, 756–765, (2000).

[8] H. Hu and R.G. Larson, Langmuir **21**, 9, 3963–3971, (2005).

[9] Y.O. Popov, Phys. Rev. E **71**, 3, 036313, (2005).

[10] H. Gelderblom, A.G. Marín, H. Nair, A. van Houselt, L. Lefferts, J.H. Snoeijer, and D. Lohse, Phys. Rev. E **83**, 2, 026306, (2011).

[11] B. Sobac and D. Brutin, Langmuir **27**, 24, 14999-15997, (2011).

[12] H. Masoud and J.D. Felske, Phys. Rev. E **79**, 1, 016301, (2009).

[13] R. Deegan, Phys. Rev. E **61**, 1, 475–485, (2000).

[14] P.L. Kelly-Zion, C.J. Pursell, S. Vaidya, and J. Batra, Colloids and Surf. A: Physicochem. Eng. Aspects **381**, 1–3, 31–36, (2011).

[15] S. David, K. Sefiane, and L. Tadrist, Colloids and Surf. A: Physicochem. Eng. Aspects **298**, 1–2, 108–114, (2007).

[16] W.D. Ristenpart, P.G. Kim, C. Domingues, J. Wan and H.A. Stone, Phys. Rev. Lett. **99**, 23, 234502.

[17] G.J. Dunn, S.K. Wilson, B.R. Duffy, S. David, and K. Sefiane, Colloids and Surf. A: Physicochem. Eng. Aspects **323**, 1–3, 50–55, (2008).

[18] G.J. Dunn, S.K. Wilson, B.R. Duffy, S. David, and K. Sefiane, J. Fluid Mech. **623**, 329–351, (2009).

[19] K. Sefiane and R. Bennacer, J. Fluid Mech. **667**, 260–271, (2011).

[20] A.J. Petsi and V.N. Burganos, Phys. Rev. E **73**, 4, 041201, (2006).

[21] D.O.H. Teare, D.C. Barwick, W.C.E. Schofield, R.P. Garrod, L.J. Ward and J.P.S. Badyal, Langmuir, **21**, 24, 11425–11430, (2005).

[22] I. Woodward, W.C.E. Schofield, V. Roucoules, and J.P.S. Badyal, Langmuir **19**, 8, 3432–3438, (2003).

[23] R. Good and M. Koo, J. Colloid Interf. Sci. **71**, 2, 283–292, (1979).

[24] P.S. Brown, A. Berson, E.L. Talbot, T.J. Wood, W.C.E. Schofield, C.D. Bain, and J.P.S. Badyal, Langmuir **27**, 22, 13897–13903, (2011).

[25] See Supplemental Material at [URL will be inserted by publisher] for videos of a pinned droplet drying on substrate G, a de-pinning droplet drying on substrate S4 and an example image sequence from the post-processing routine.